iScience

CellPress
OPEN ACCESS

Article

A parasite outbreak in notothenioid fish in an Antarctic fjord

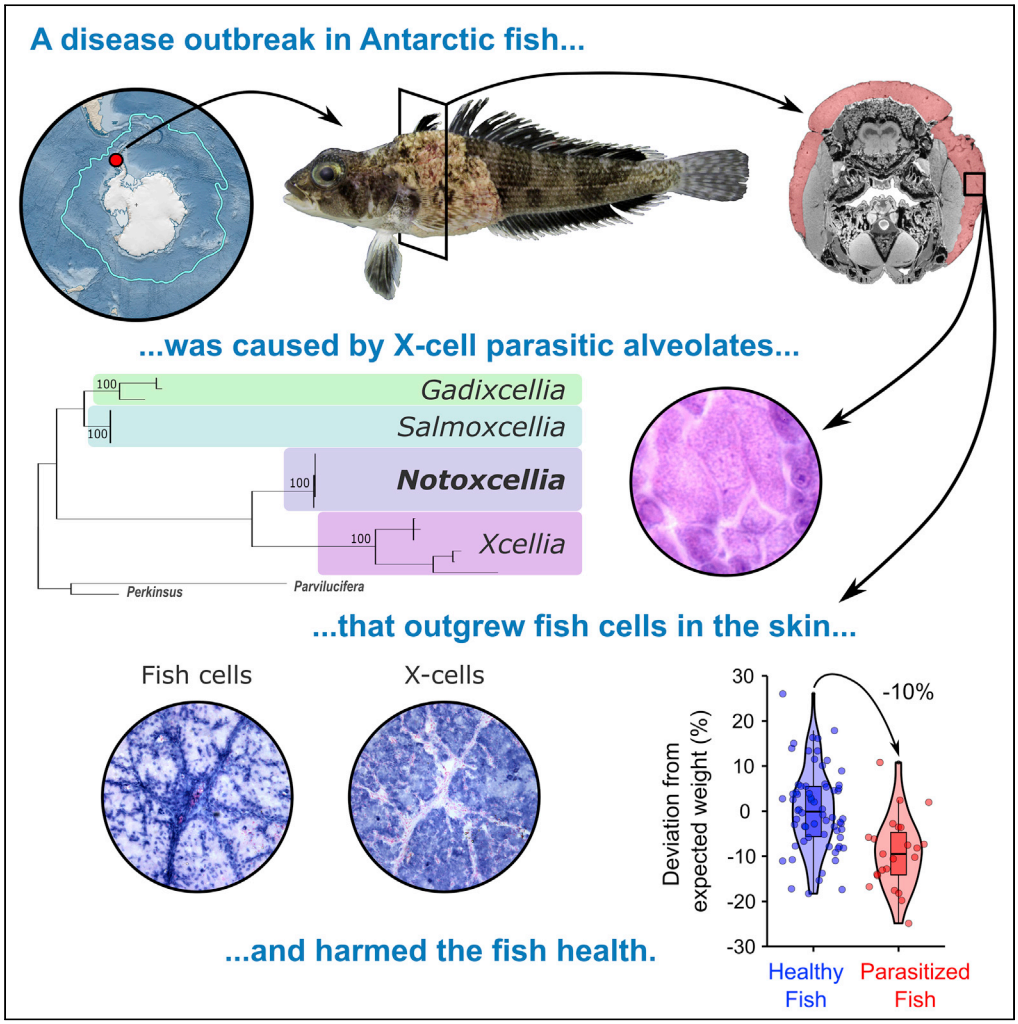

Thomas Desvignes, Henrik Lauridsen, Alejandro Valdivieso, ..., Michael L. Kent, Arvind Varsani, John H. Postlethwait

tdesvign@uoregon.edu (T.D.)
arvind.varsani@asu.edu (A.V.)
jpostle@uoregon.edu (J.H.P.)

Highlights

A worrisome disease outbreak affected fish in an Antarctic Peninsula fjord

A parasitic alveolate in the Xcellidae family caused large skin tumors

We describe the genus *Notoxcellia* with two species, *Notoxcellia coronata* and *N. picta*

These parasites have detrimental effects on fish host physiology and health

Desvignes et al., iScience *25*, 104588
July 15, 2022
https://doi.org/10.1016/j.isci.2022.104588

iScience

CellPress
OPEN ACCESS

Article

A parasite outbreak in notothenioid fish in an Antarctic fjord

Thomas Desvignes,[1,10,*] Henrik Lauridsen,[2] Alejandro Valdivieso,[3,9] Rafaela S. Fontenele,[4] Simona Kraberger,[4] Katrina N. Murray,[1] Nathalie R. Le François,[5] H. William Detrich III,[6] Michael L. Kent,[7] Arvind Varsani,[4,8,*] and John H. Postlethwait[1,*]

SUMMARY

Climate changes can promote disease outbreaks, but their nature and potential impacts in remote areas have received little attention. In a hot spot of biodiversity on the West Antarctic Peninsula, which faces among the fastest changing climates on Earth, we captured specimens of two notothenioid fish species affected by large skin tumors at an incidence never before observed in the Southern Ocean. Molecular and histopathological analyses revealed that X-cell parasitic alveolates, members of a genus we call *Notoxcellia*, are the etiological agent of these tumors. Parasite-specific molecular probes showed that xenomas remained within the skin but largely outgrew host cells in the dermis. We further observed that tumors induced neovascularization in underlying tissue and detrimentally affected host growth and condition. Although many knowledge gaps persist about X-cell disease, including its mode of transmission and life cycle, these findings reveal potentially active biotic threats to vulnerable Antarctic ecosystems.

INTRODUCTION

Waters of the Southern Ocean have been environmentally stable and chronically cold, hovering near the freezing point for the past 15–20 million years. The climate in Antarctica, however, is rapidly changing (CNRS, LOCEAN-IPSL and Sallée, 2018; Convey and Peck, 2019; Morley et al., 2020), with rising air temperatures and melting glaciers contributing to warmer and fresher bottom waters (Rye et al., 2020; Silvano et al., 2018; Swart et al., 2018). Strong abiotic stressors are already affecting the highly endemic and specialized Antarctic fauna (Brasier et al., 2021; Caccavo et al., 2021; Gutt et al., 2021), causing a cascade of responses from molecular to community levels. The integration of these perturbations on species interactions, however, remains poorly understood.

The Antarctic fish fauna is dominated by the sub-order Notothenioidei, a rare example of a marine species flock (Chenuil et al., 2018). Within this flock, the white-blooded icefishes represent true evolutionarily oddities, possessing adaptations that appear to help compensate for their unique lack of functional hemoglobin (Beck et al., 2022; Kim et al., 2019). Physiological responses of Antarctic fish to abiotic stressors, including temperature change, reveal lengthy acclimation periods (Davis et al., 2018; Enzor et al., 2017; Peck, 2018), raising concerns about their resilience and vulnerability due to slow growth, long lives, and low fecundity (Mesa and Vacchi, 2001). Biotic stressors, including changing microbial and viral community dynamics (Clark et al., 2019; Danovaro et al., 2011; Pinkerton et al., 2021), are also likely to become more prevalent and may bring species to a tipping point (Cohen et al., 2020; Price et al., 2019). We have limited knowledge, however, of present and emerging biotic threats in remote regions and extreme environments on our planet.

RESULTS

A disease outbreak in Antarctic fishes

While conducting research operations in Andvord Bay, a hot spot of biodiversity on the West Antarctic Peninsula near the Palmer Archipelago (Grange and Smith, 2013) during the austral fall 2018 (Figure 1A), we captured many specimens of crowned notothen *Trematomus scotti*, of which ~30% displayed large skin tumors or tissue masses (Figure 1B). Tumors were pale pink, raised, rough, and appeared at various places on the trunk and head, in some cases covering more than a third of the body surface (Figure S1).

[1]Institute of Neuroscience, University of Oregon, Eugene, OR 97403, USA

[2]Department of Clinical Medicine, Aarhus University; Palle Juul-Jensens Boulevard 99, 8200 Aarhus N, Denmark

[3]Institut de Ciències del Mar, Consejo Superior de Investigaciones Científicas (CSIC), Barcelona Spain

[4]The Biodesign Center for Fundamental and Applied Microbiomics, Center for Evolution and Medicine and School of Life Sciences, Arizona State University, Tempe, AZ 85287, USA

[5]Laboratoire Physiologie, Aquaculture et Conservation, Biodôme de Montréal/Espace pour la vie, 4777 Avenue Pierre-De Coubertin, Montreal, QC H1V 1B3, Canada

[6]Department of Marine and Environmental Sciences, Northeastern University Marine Science Center, 430 Nahant Rd, Nahant, MA 01908, USA

[7]Department of Microbiology, Oregon State University, Corvallis, OR 97331, USA

[8]Structural Biology Research Unit, Department of Integrative Biomedical Sciences, University of Cape Town, 7925 Cape Town, South Africa

[9]Present address: IHPE, CNRS, IFREMER, Université de Montpellier, 34090 Montpellier, France

[10]Lead contact

*Correspondence: tdesvign@uoregon.edu (T.D.), arvind.varsani@asu.edu (A.V.), jpostle@uoregon.edu (J.H.P.)

https://doi.org/10.1016/j.isci.2022.104588

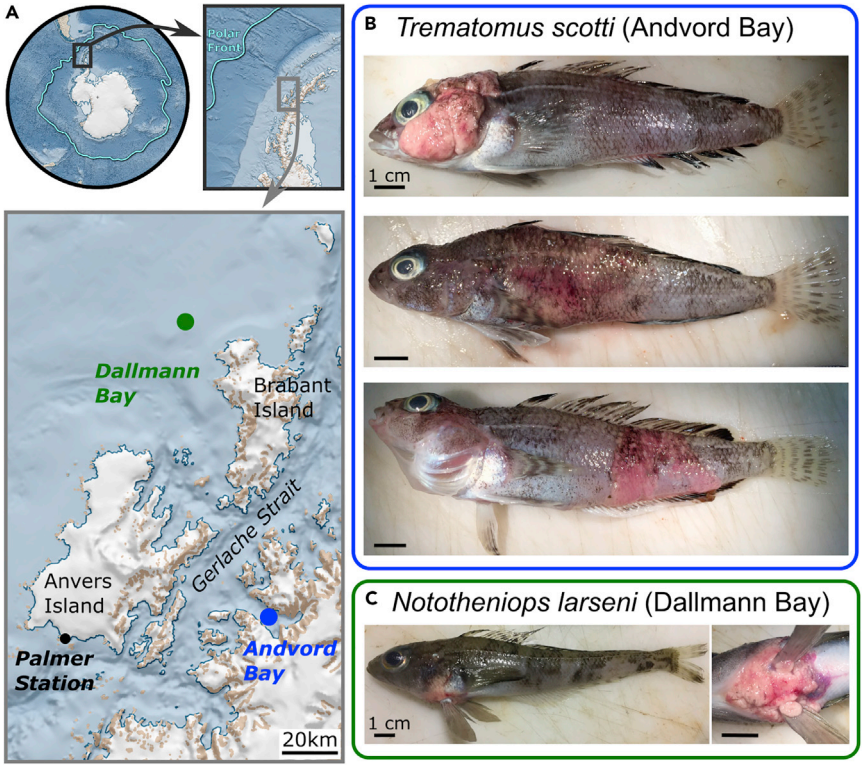

Figure 1. Capture locations and affected Antarctic notothenioid specimens

(A) Animal collection sites. The cyan line marks the Polar Front.

(B) Three specimens of crowned notothen *Trematomus scotti* from Andvord Bay and (C) a painted notothen *Nototheniops larseni* from Dallmann Bay. Tumors in *T. scotti* affected skin anywhere on the body. Tumors in *N. larseni* developed below the head and between the pelvic fins. See also Figure S1.

Field examinations suggested that tumors were restricted to the skin (Figure S2A). Our similar fishing operations four years earlier at the same location and season detected no affected fish despite capturing hundreds of crowned notothens (Figure S2B). Furthermore, of 14 international long-term Antarctic fish researchers, we contacted about these pathologic observations, only four reported having ever seen such lesions, always in few fish (Data S1). We conclude that the situation observed in 2018 constitutes a recent outbreak of a pathogenic agent that may have been present, but rarely affected fish in Antarctic waters in the past.

A few weeks later near Dallmann Bay, approximately 100 km north of Andvord Bay, we captured a painted notothen *Nototheniops larseni*, one of hundreds captured that season, that was affected by similar skin tumors under the head and between the pelvic fins (Figure 1C). The external and erythemic phenotype of the tumor in this painted notothen, however, differed substantially from the non-erythemic and more rugose phenotype of tumors observed in crowned notothens.

Logistical constraints prevented us from preserving and analyzing the hundreds of specimens of crowned notothen captured that night in Andvord Bay. Nonetheless, to investigate the etiology and pathology of their skin tumors, we randomly retained 66 apparently healthy and 24 diseased crowned notothens. We also examined the single diseased painted notothen paired with an apparently healthy conspecific control.

Unicellular parasites cause the disease

Oncogenic viruses (polyomaviruses and papillomaviruses) have recently been identified in notothenioids in the Ross Sea (East Antarctica) (Buck et al., 2016; Kraberger et al., 2022; Van Doorslaer et al., 2018). To test the hypothesis that a virus caused these tumors, we conducted a metagenomic analysis on tumors of five crowned notothens and the diseased painted notothen and compared results to those from visually healthy

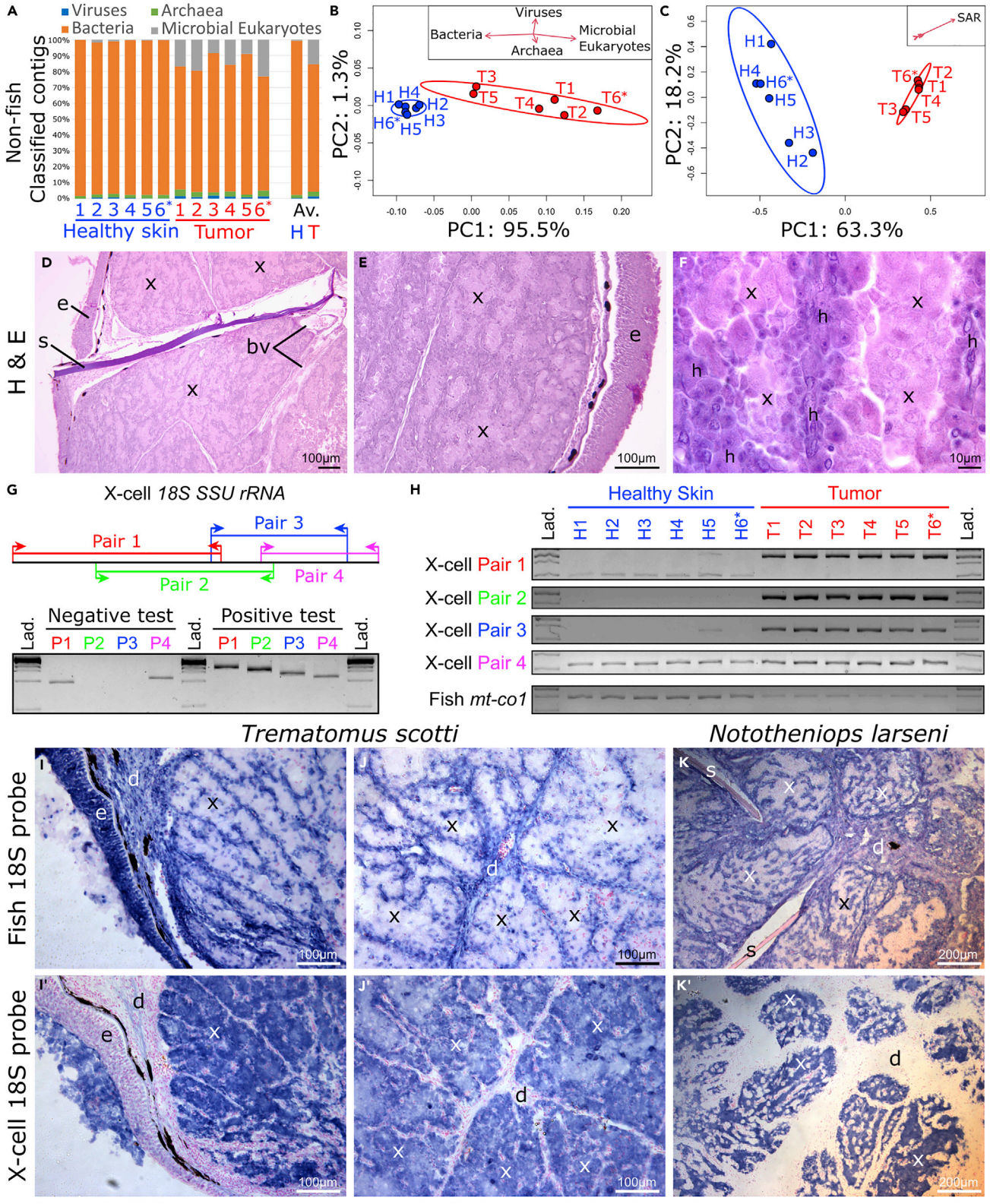
A
Viruses
Archaea
Bacteria
Microbial Eukaryotes
Non-fish Classified contigs
100%
90%
80%
70%
60%
50%
40%
30%
20%
10%
0%
1 2 3 4 5 6* 1 2 3 4 5 6* Av.
Healthy skin Tumor H T
B
Viruses
Bacteria
Microbial Eukaryotes
Archaea
PC2: 1.3%
PC1: 95.5%
C
SAR
PC2: 18.2%
PC1: 63.3%
D
E
F
H & E
bv
100µm
10µm
G
X-cell 18S SSU rRNA
Pair 1
Pair 2
Pair 3
Pair 4
Negative test
Positive test
Lad.
P1 P2 P3 P4
H
Healthy Skin
Tumor
X-cell Pair 1
X-cell Pair 2
X-cell Pair 3
X-cell Pair 4
Fish mt-co1
Trematomus scotti
Nototheniops larseni
Fish 18S probe
X-cell 18S probe
200µm

Figure 2. Tumors are X-cell xenomas

(A) Proportions and (B) principal coordinates analysis (PCoA) of taxonomically classified non-fish contigs in apparently healthy skin (H, blue) and tumors (T, red) revealed abundant microbial eukaryotes in tumors. Inserts in B and C indicate contributions of variables. Asterisks (*) denote samples from *Nototheniops larseni*.

(C) PCoA of taxonomically classified microbial eukaryote contigs demonstrated that SAR contigs distinguished healthy skin (n = 6) from tumors (n = 6). Contributions of other groups are not visible at this scale. See also Figure S3.

(D–F) Histopathology revealed parasites similar to X-cells in tumors. See also Figure S4.

(G) PCR tests can identify X-cell parasites. See also Data S2.

(H) PCR showed DNA of X-cells in tumors and their absence from apparently healthy skin, except for "healthy" sample H5. PCR amplification of fish mitochondrial marker *mt-co1* showed low quantities of fish DNA in tumors.

(I–K) *In situ* hybridization for 18S rRNAs of the fish host or (I'-K') X-cell parasites in adjacent sections confirmed abundant X-cells in tumors and revealed xenoma structure, showing reciprocal staining of parasites in compartments with thin walls of fish cells. See also Figure S5. Av., average across biological replicates. bv, blood vessel; d, dermis; e, epidermis; h, host cells; Lad., ladder; s, scale; x, xenoma.

skin from five crowned notothens and one painted notothen. We did not detect any abundant DNA or RNA virus sequences in any sample, suggesting an alternative etiology for the observed pathologic changes. Taxonomic classification of DNA sequences of assembled metagenomic contigs, however, revealed an over-abundance of microbial eukaryotic DNA in tumors compared to apparently healthy skin samples (Figures 2A, 2B, S3A, and S3B). Among microbial eukaryotes, the SAR clade (Stramenopile, Alveaolata, Rhizaria) drove the separation of tumor vs. healthy skin samples (Figures 2C, S3C, and S3D), suggesting that a member of the SAR clade caused the tumors.

To determine whether tumors were invasive and to understand tumor histopathology, we examined histological sections of affected skin. Results revealed massive growths in the dermis that encompassed scales (Figures 2D and S4). Tumors contained large, basophilic cells with indistinct nuclei filling compartments lined by small cells (Figure 2E). The large cells were histologically similar to those previously identified in X-cell disease (Bucke and Everson, 1992; Freeman et al., 2017), whereas the smaller cells resembled host fibroblasts, together forming multiple xenoparasitic complexes (Figure 2F). X-cell disease affects various fish groups throughout the world (Bucke and Everson, 1992; Davison, 1997; Diamant et al., 1994; Evans and Tupmongkol, 2014; Freeman et al., 2011, 2017; Freeman, 2009; Karlsbakk et al., 2021; Miwa and Kamaishi, 2009) and is caused by a parasitic alveolate of the family Xcellidae that is related to the bivalve parasite *Perkinsus* (Freeman et al., 2017; Itoïz et al., 2022).

All five tumor metagenomic samples contained Xcellidae-related 18S rRNA contigs but four of five visually healthy skins did not, the exception being sample H5 from an otherwise apparently healthy fish. Using existing (Freeman, 2009; Freeman et al., 2017; Hillis and Dixon, 1991) and new PCR primers, we developed a molecular assay specifically designed to amplify the 18S SSU (small subunit) rRNA gene of all known Xcellidae species with available genomic resources (Figure 2G and Data S2). Using this diagnostic tool, we confirmed the presence of Xcellidae DNA in all tumor samples used for metagenomic analysis and its absence from visually healthy samples other than H5 (Figure 2H and Data S2). As a control, we amplified the notothenioid mitochondrial marker *mt-co1* in the same DNA extracts and confirmed the presence of fish mtDNA in all samples. Even though the amount of template DNA was constant among PCR assays, fish *mt-co1* signal was faint in tumors compared to healthy skin (Figure 2H), as expected if a large proportion of DNA extracted from tumors was not fish DNA.

Notoxcellia, a previously unknown parasite genus

Our metagenomic analysis assembled multiple-kilobase long fragments of DNA containing the X-cell parasite 18S rRNA genes for each xenoma sample of both crowned and painted notothens. Phylogenetic reconstructions using a variety of alveolate 18S SSU rRNA sequences placed all tumor sequences within the Xcellidae family (Figure 3), which contains three described genera, *Gadixcellia*, *Salmoxcellia*, and *Xcellia* (Freeman et al., 2017; Karlsbakk et al., 2021). All of our notothen-derived sequences, however, occupied a long branch distinct from previously identified genera (Figure 3B), supporting the conclusion that Xcellidae parasites infecting crowned and painted notothens belong to a different genus, which we call *Notoxcellia* to reference the type hosts (Data S3). X-cell disease was previously reported in gills of four species of Antarctic notothens from McMurdo Sound in the Ross Sea (Davison, 1997; Evans and Tupmongkol, 2014; Franklin and Davison, 1988). Our phylogenetic analysis revealed that the parasite infecting one of the previously reported notothens (Evans and Tupmongkol, 2014) was in the genus *Xcellia* (Figure 3B), not *Notoxcellia*. Furthermore, these previously reported *Xcellia* infected gills, not skin as in our samples. In the gray notothen *Lepidonotothen squamifrons*, however, large X-cell

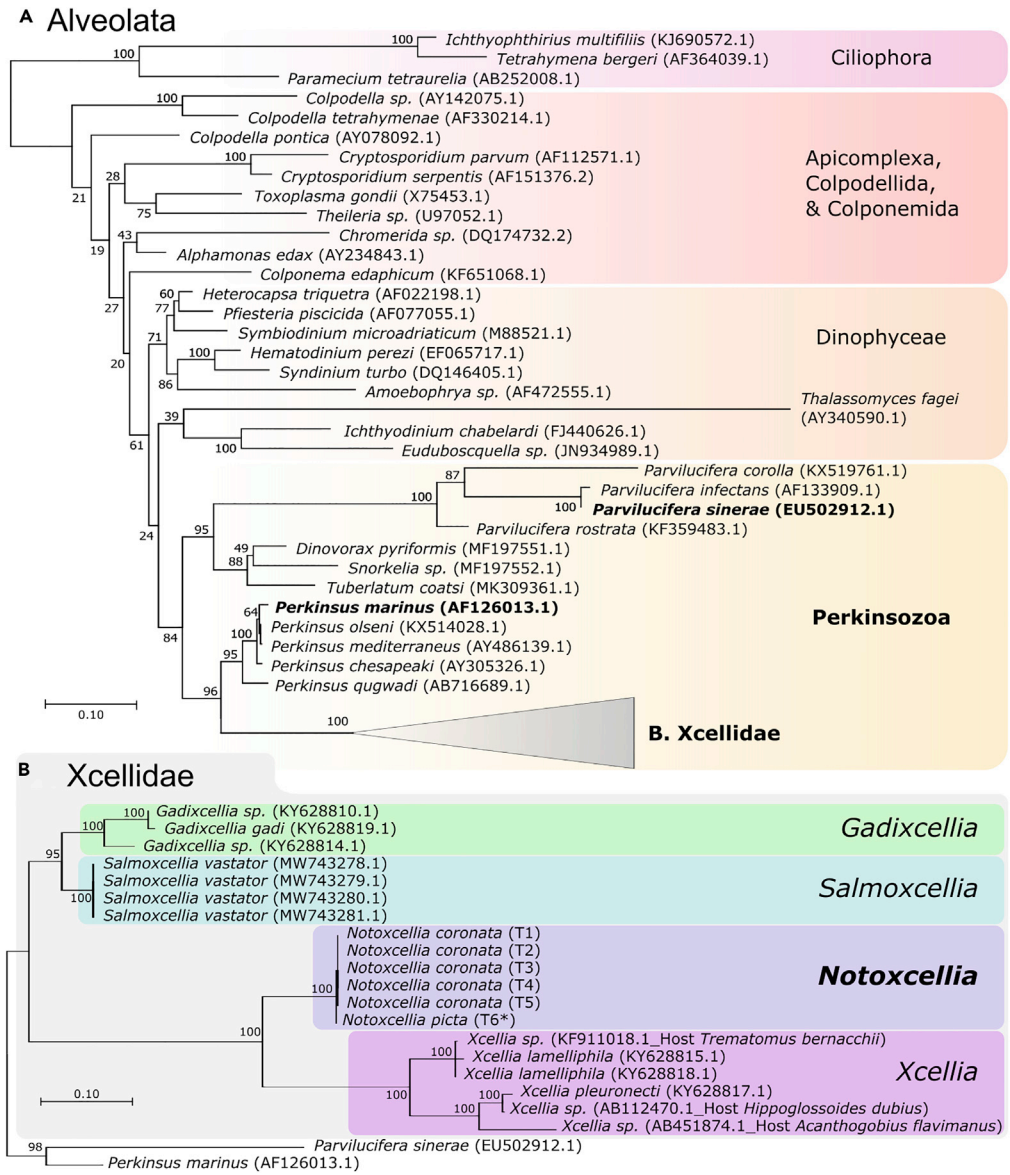

Figure 3. Phylogenetic placement of *Notoxcellia* species

(A) Phylogenetic reconstruction of major alveolate species places the parasite samples we identified within the Xcellidae family, within Perkinsozoa.

(B) Within Xcellidae, notothenioid X-cell sequences grouped in a long branch well individualized from the previously described *Gadixcellia*, *Salmoxcellia*, and *Xcellia* genera, supporting the description of the genus *Notoxcellia*. The perfect identity of all *Notoxcellia* sequences among the five crowned notothen studied (T1-T5) and their genetic divergence from the *Notoxcellia* sequence of the painted notothen (T6*) support two different *Notoxcellia* species. Scale bars represent a substitution rate of 0.1 nucleotide per site. See also Data S3.

skin lesions were reported once in 1992 on five fish captured around South Georgia (Bucke and Everson, 1992), but resources are unavailable for molecular characterization. These results demonstrate that multiple Xcellidae taxa are present in the Southern Ocean and may be evolving to parasitize different organs and hosts. Furthermore, *Notoxcellia* sequences from our five infected crowned notothens were identical and clustered closely with the sequence from the infected painted notothen, although diverging by 1.64% over 14.5 kb (Figure 3B and Data S3), indicating that parasites from the two different hosts are separate species within the genus *Notoxcellia*. We thus describe two *Notoxcellia* species: *N. coronata* in the type host crowned notothen and *N. picta* in the type host painted notothen (Data S3).

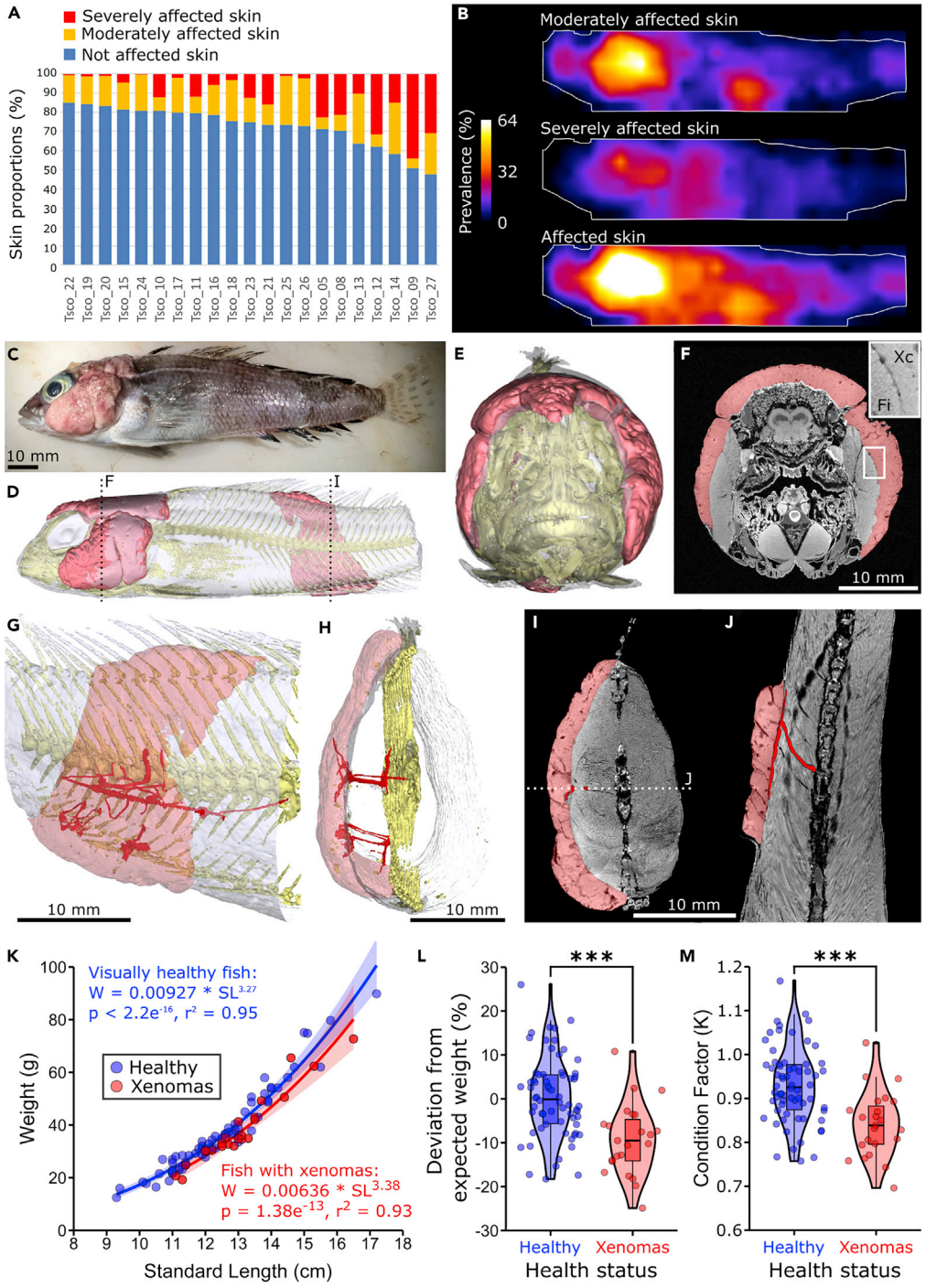

Figure 4. Pathology of X-cell infection

(A) Proportion of skin visually healthy (blue), moderately affected (yellow), or severely affected (red).

(B) X-cell infection prevalence maps on crowned notothens (n = 21). The white outline represents the average fish shape in lateral view, head on the left, dorsal side up. See also Figure S6.

(C–E) Image of a crowned notothen analyzed by microMRI and resulting segmented 3D model in (D) left-side and (E) face-on views. The fish skeleton is represented in yellow and xenomas in pink.

(F) MRI slice through the head as positioned by a dotted line in (D) shows that the xenoma did not invade internal organs. In insert, Fi labels fish tissue and Xc, X-cells.

Figure 4. *Continued*

(G and H) Segmented model of tail region showing in deep red enlarged intersegmental blood vessels irrigating xenomas.

(I and J) Individual MRI slices illustrating segmental blood vessels. See also Figure S7, Datas S4 and S5, Videos S1 and S2.

(K–M) Fish with xenomas (n = 23) displayed a lower growth model than apparently healthy fish (n = 66) (represented with 95% CI), resulting in fish with xenomas (L) being on average 10% lighter than their expected weight (one-sided *t-test*, $t = 4.73$, $df = 43.2$, $p = 1.22 \times 10^{-5}$) and (M) having a significantly lower condition factor (one-sided *t-test*, $t = 4.73$, $df = 43.2$, $p = 1.22 \times 10^{-5}$). Boxplots in L and M represent the median, 25th and 75th percentiles, and 1.5x IQR. The dots plotted in K–M represent data points for individual fish. See also Figure S8 and Data S6.

Pathology of X-cell infection

To distinguish fish cells from X-cells in xenomas and to determine their organization, we performed *in situ* hybridization experiments on adjacent histological sections with species-specific probes for *Notoxcellia* and fish host 18S SSU rRNAs. Results showed that the fish probe labeled thin partitions delineating open compartments (Figures 2I, 2J, and S5). In contrast, the *Notoxcellia* probe labeled cells filling open spaces between the partitions identified by the fish probe (Figures 2I′–J′ and S5); each image was the negative of the other. These hybridization experiments show that these xenomas are macroscopically visible masses comprised of host and parasitic cells. *In situ* hybridization further showed that the overall arrangement of the xenomas was relatively similar in the two fish species, but differed with respect to the organization of host lamellae, which appeared thicker and delineated well-individualized xenoparasitic complexes in the painted notothen (Figures 2K–2K′ and S5). These differences might be due to differences in the sites of infection (pelvic region vs. flanks) or the general response of the host to infection, but perhaps also to different modes of parasitic growth of the two *Notoxcellia* species.

To study how *Notoxcellia* parasitizes different body parts, we scored the distribution of lesions on the fish. Using images of both sides of 21 affected crowned notothens and a randomized point grid, we categorized skin as healthy, moderately affected, or severely affected (Figure S6A). Results revealed substantial variation, ranging from individuals with only 15% of moderately affected skin to those with about 50% of mostly severely affected skin (Figure 4A). While left and right sides were not significantly different (paired *t-test*, $t = -0.65$, $df = 20$, $p = 0.52$, Figure S6B) and xenomas were found anywhere on the body, skin at the back of the head near the operculum and posterior to the anus was more frequently affected (Figures 4B and S6C). These xenoma hot spots suggest that initial infection could be linked to ingestion, respiration, and excretion. Variation in the amount of affected skin and xenoma location might also be influenced by the general health of the fish at infection, its age, and time elapsed since infection. Furthermore, because our metagenomic data, verified by PCR, showed that visually healthy skin could already be invisibly parasitized by *Notoxcellia* (Figure 2H), it is likely that the proportion of parasitized skin, as well as the number of specimens already infected, was higher than initial estimates.

Using three specimens, we analyzed the 3-dimensional nature of severe lesions by microMRI and microCT. Results showed that xenomas were morphologically distinct from the rest of the body and remained superficial, within the skin, without invading underlying tissues (Figures 4C–4F and S7, Data S4 and S5, Videos S1 and S2). Nonetheless, xenomas could grow to encompass 8% of the fish's total volume (Figure S7C). In one specimen, xenomas covered up to 270° around the fish head (Figures 4E and 4F). A second mass, seemingly independent, burst out on the right flank. Analysis of interactions of the xenoma with the underlying musculature revealed the remodeling of myosepta into cavities that appear to be enlarged intersegmental blood vessels vascularizing the parasitic mass in the dermis (Figures 4G–4J and S7D–S7G, Data S5 and Video S2).

Consequences of X-cell infection

Growth and body condition can reveal an individual's resilience to stressors. Comparing morphological data from diseased and apparently healthy crowned notothens caught in the same trawls, we observed that diseased fish had significantly lower total weight and Fulton's condition factor than healthy fish (one-sided *t-test*, $t = 4.73$, $df = 43.2$, $p = 1.22 \times 10^{-5}$): fish with xenomas were on average 10% lighter than their expected weight based on their length (one-sided *t-test*, $t = -4.73$, $df = 43.2$, $p = 1.22 \times 10^{-5}$, Figures 4K–4M and S8 and Data S6). X-cell infection in Antarctic bald notothen *Trematomus borchgrevinki* showed similar results (Davison, 1997). We conclude that *Notoxcellia* negatively impacts the host's health.

DISCUSSION

These molecular-genetic, phylogenetic, histopathological, and *in situ* hybridization analyses together showed that skin tumors identified in two Antarctic fish species were caused by the alveolates *Notoxcellia* spp., closely related to, but distinct from, previously known X-cell parasites (Freeman et al., 2017; Karlsbakk et al., 2021). Our studies further revealed that *Notoxcellia*, which proliferates within the dermis of the fish host in compartments between thin walls of host cells, has detrimental effects on host condition. Given the severity of the lesions, their effect on fish growth, and the long lives of Antarctic notothenioids (up to 22 years for crowned notothens (Mesa and Vacchi, 2001)), these parasite infections are likely to reduce the fitness of affected fish.

Many knowledge gaps persist about X-cell disease, including the life cycle of X-cell parasites (Freeman et al., 2011), confirmation of their possible transmission by contact of the fish with the benthic substrate (Freeman et al., 2017), potential biotic and abiotic reservoirs, host ranges (i.e., the number of host species for a given parasite species), host-parasite interactions, and biogeographic distribution of the various X-cell lineages (Itoïz et al., 2022). It cannot be excluded, however, that the outbreak may expand within this population, spread to other localities, and potentially infect other species. X-cell disease occurrence appears extremely variable and inconsistent, with patchy geographical distributions that can vary dramatically over the years (Diamant and Mcvicar, 1990; Freeman et al., 2017; Karlsbakk et al., 2021; Mellergaard and Nielsen, 1996), including in Antarctica (Davison, 1997). It is thus possible that similar epidemics have occurred in the past and escaped detection by careful observers who can explore only a small fraction of the Southern Ocean. Physical environmental factors such as natural climatic cycles and biological factors that result in periodic high infection rates could explain our uncommon observations. Although sea bottom temperatures at our capture sites were not dramatically different than those at other nearby localities (Figure S9), glaciers on the West Antarctic Peninsula are melting at a rapid pace, affecting Antarctic bottom waters, which have warmed and freshened for several decades (Rye et al., 2020; Silvano et al., 2018; Swart et al., 2018). The warmer, fresher Antarctic shelf water may act on *Notoxcellia* to improve its dispersion or infectivity. It is also possible that these changes act detrimentally on fish physiology, weakening individuals so that they become more prone to infection. While we currently lack the data and knowledge to predict how X-cells might be affected by global climate change, with alarming forecasts for continued changes in Antarctic climates (IPCC, 2021), this dramatic situation in this population may forecast large-scale biotic changes in host-parasite interactions triggered by changes in the abiotic environment. Additional field surveys and awareness of the scientific community are urgently needed to better understand the current epidemic context of the Southern Ocean and reveal how global climate change, natural biotic and abiotic processes, and other anthropogenic activities might affect the virulence and transmission of these X-cell parasites in Antarctic notothenioids and other fishes.

Limitations of the study

Noticing the severe tumors in crowned notothens immediately after recovery of both trawls, we decided not to collect all diseased specimens due to concerns about transporting potentially contagious pathogens to the aquarium facilities at Palmer Station and its surrounding environment. While our selection of specimens to study was not motivated by any criteria, it is possible that we unconsciously biased sampling toward larger specimens or severely affected specimens. Therefore, our sampling may not precisely reflect the prevalence of tumors in the population.

A second limitation of the study concerns a possible link between this disease outbreak and changes to the environment. While we currently lack the data and knowledge necessary to predict how global climate change might affect X-cells or the disease they cause, it is likely that changes to the environment would affect the ecology and epidemiology of this parasite. To monitor the prevalence of X-cell disease in Antarctica and link its incidence to environmental change, despite major logistical constraints, additional and repeated field campaigns are necessary over time. In this context, broad international scientific community awareness and participation is required to collectively draw a clearer picture of X-cell disease prevalence around the Antarctic continent, and more broadly shed light on the pathogenic context in the Southern Ocean. The diagnostic tests our work provides can contribute to these endeavors.

STAR★METHODS

Detailed methods are provided in the online version of this paper and include the following:

- KEY RESOURCES TABLE
- RESOURCE AVAILABILITY
  - Lead contact
  - Materials availability
  - Data and code availability
- EXPERIMENTAL MODEL AND SUBJECT DETAILS
- METHOD DETAILS
  - Metagenomic analysis
  - Histopathology
  - PCR amplifications
  - Phylogenetic tree reconstruction
  - *In situ* hybridization
  - Surface analysis
  - microMRI and microCT analyses
  - Morphometric analyses
- QUANTIFICATION AND STATISTICAL ANALYSIS

SUPPLEMENTAL INFORMATION

Supplemental information can be found online at https://doi.org/10.1016/j.isci.2022.104588.

ACKNOWLEDGMENTS

We thank the captain and crew of the *ARSV Laurence M. Gould*, the personnel of the U.S. Antarctic Program for assistance in Chile, at sea, and at Palmer Station, as well as the logistics in Denver, CO for their support related to the Antarctic fieldwork required for this study. We also thank the University of Oregon Fish Histology Group. We are grateful for our Antarctic fish research colleagues who responded with surprise, interest, and concerns after we contacted them about this pathologic outbreak. Contribution [423] from the Marine Science Center at Northeastern University. The work behind this scientific publication inspired a short scientific graphic novel *A mysterious disease in Antarctic fish* publicly available at https://blogs.uoregon.edu/antarcticxcell/. This work was funded by the National Science Foundation grants OPP-1947040 (JHP and ArV), PLR-1444167 (HWD), and OPP-1543383 (JHP, TD, and HWD).

AUTHOR CONTRIBUTIONS

Conceptualization: TD, HL, ArV, JHP, Field Work: JHP, TD, HL, NRLF, Data curation: TD, HL, ArV, Formal Analysis: TD, HL, AlV, RSF, SK, Funding acquisition: JHP, TD, ArV, HWD, Investigation: TD, HL, AlV, RSF, SK, KNM, NRLF, MLK, JHP, Methodology: TD, HL, AlV, Project administration: TD, ArV, JHP, Resources: TD, HL, HWD, ArV, JHP, Supervision: TD, ArV, JHP, Validation: TD, ArV, JHP, Visualization: TD, HL, AlV, JHP, Writing – original draft: TD, JHP, Writing – review & editing: TD, HL, AlV, RSF, SK, KNM, NRLF, HWD, MLK, ArV, JHP.

DECLARATION OF INTERESTS

The authors declare no competing interests.

INCLUSION AND DIVERSITY

One or more of the authors of this paper self-identifies as an underrepresented ethnic minority in science. One or more of the authors of this paper self-identifies as a member of the LGBTQ+ community. While citing references scientifically relevant for this work, we also actively worked to promote gender balance in our reference list.

Received: April 29, 2022
Revised: May 25, 2022
Accepted: June 7, 2022
Published: July 15, 2022

REFERENCES

Beck, E.A., Healey, H.M., Small, C.M., Currey, M.C., Desvignes, T., Cresko, W.A., and Postlethwait, J.H. (2022). Advancing human disease research with fish evolutionary mutant models. Trends Genet. *38*, 22–44. https://doi.org/10.1016/j.tig.2021.07.002.

Bolger, A.M., Lohse, M., and Usadel, B. (2014). Trimmomatic: a flexible trimmer for Illumina sequence data. Bioinformatics *30*, 2114–2120. https://doi.org/10.1093/bioinformatics/btu170.

Brasier, M.J., Barnes, D., Bax, N., Brandt, A., Christianson, A.B., Constable, A.J., Downey, R., Figuerola, B., Griffiths, H., Gutt, J., et al. (2021). Responses of Southern Ocean seafloor habitats and communities to global and local drivers of change. Front. Mar. Sci. *8*, 109. https://doi.org/10.3389/fmars.2021.622721.

Buck, C.B., Van Doorslaer, K., Peretti, A., Geoghegan, E.M., Tisza, M.J., An, P., Katz, J.P., Pipas, J.M., McBride, A.A., Camus, A.C., et al. (2016). The ancient evolutionary history of polyomaviruses. PLoS Pathog. *12*, e1005574. https://doi.org/10.1371/journal.ppat.1005574.

Bucke, D., and Everson, I. (1992). "X-cell" lesions in notothenia (lepidonotothen) squamifrons gunther. Bull. Eur. Assoc. Fish Pathol. *12*, 83–86.

Caccavo, J.A., Christiansen, H., Constable, A.J., Ghigliotti, L., Trebilco, R., Brooks, C.M., Cotte, C., Desvignes, T., Dornan, T., Jones, C.D., et al. (2021). Productivity and change in fish and squid in the Southern Ocean. Front. Ecol. Evol. *9*. https://doi.org/10.3389/fevo.2021.624918.

Chenuil, A., Saucède, T., Hemery, L.G., Eléaume, M., Féral, J.P., Améziane, N., David, B., Lecointre, G., and Havermans, C. (2018). Understanding processes at the origin of species flocks with a focus on the marine Antarctic fauna. Biol. Rev. *93*, 481–504. https://doi.org/10.1111/brv.12354.

Clark, M.S., Villota Nieva, L., Hoffman, J.I., Davies, A.J., Trivedi, U.H., Turner, F., Ashton, G.V., and Peck, L.S. (2019). Lack of long-term acclimation in Antarctic encrusting species suggests vulnerability to warming. Nat. Commun. *10*, 3383. https://doi.org/10.1038/s41467-019-11348-w.

CNRS, LOCEAN-IPSL, and Sallée, J.-B. (2018). Southern Ocean Warming. Oceanography *31*. https://doi.org/10.5670/oceanog.2018.215.

Cohen, J.M., Sauer, E.L., Santiago, O., Spencer, S., and Rohr, J.R. (2020). Divergent impacts of warming weather on wildlife disease risk across climates. Science *370*, eabb1702. https://doi.org/10.1126/science.abb1702.

Convey, P., and Peck, L.S. (2019). Antarctic environmental change and biological responses. Sci. Adv. *5*, eaaz0888. https://doi.org/10.1126/sciadv.aaz0888.

Criscuolo, A., and Gribaldo, S. (2010). BMGE (Block Mapping and Gathering with Entropy): a new software for selection of phylogenetic informative regions from multiple sequence alignments. BMC Evol. Biol. *10*, 210. https://doi.org/10.1186/1471-2148-10-210.

Danovaro, R., Corinaldesi, C., Dell'Anno, A., Fuhrman, J.A., Middelburg, J.J., Noble, R.T., and Suttle, C.A. (2011). Marine viruses and global climate change. FEMS Microbiol. Rev. *35*, 993–1034. https://doi.org/10.1111/j.1574-6976.2010.00258.x.

Davis, B.E., Flynn, E.E., Miller, N.A., Nelson, F.A., Fangue, N.A., and Todgham, A.E. (2018). Antarctic emerald rockcod have the capacity to compensate for warming when uncoupled from CO2-acidification. Global Change Biol. *24*, e655–e670. https://doi.org/10.1111/gcb.13987.

Davison, W. (1997). X-cell gill disease in Pagothenia borchgrevinki from McMurdo Sound, Antarctica. Polar Biol. *19*, 17–23. https://doi.org/10.1007/s003000050211.

Desvignes, T., Le François, N.R., Goetz, L.C., Smith, S.S., Shusdock, K.A., Parker, S.K., Postlethwait, J.H., and Detrich, H.W. (2019). Intergeneric hybrids inform reproductive isolating barriers in the Antarctic icefish radiation. Sci. Rep. *9*, 5989. https://doi.org/10.1038/s41598-019-42354-z.

Diamant, A., Fournie, J.W., Courtney, L.A., and DiAmAnt, A. (1994). X-cell pseudotumors in a hardhead catfish Arius fells (Ariidae) from Lake Pontchartrain, Louisiana, USA. Dis. Aquat. Org. *18*, 181–185. https://doi.org/10.3354/dao018181.

Diamant, A., and Mcvicar, A.H. (1990). Distribution of X-cell disease in common dab, Limanda limanda L., in the North Sea, and ultra-structural observations of previously undescribed developmental stages. J. Fish. Dis. *13*, 25–37. https://doi.org/10.1111/j.1365-2761.1990.tb00754.x.

Dray, S., and Dufour, A.-B. (2007). The ade4 package: implementing the duality diagram for ecologists. J. Stat. Software *22*, 1–20. https://doi.org/10.18637/jss.v022.i04.

Enzor, L.A., Hunter, E.M., and Place, S.P. (2017). The effects of elevated temperature and ocean acidification on the metabolic pathways of notothenioid fish. Conserv. Physiol. *5*, cox019. https://doi.org/10.1093/conphys/cox019.

Evans, C.W., and Tupmongkol, K. (2014). X-cell disease in Antarctic fishes. Polar Biol. *37*, 1261–1269. https://doi.org/10.1007/s00300-014-1518-6.

Franklin, C.E., and Davison, W. (1988). X-cells in the gills of an Antarctic teleost, Pagothenia borchgrevinki. J. Fish. Biol. *32*, 341–353. https://doi.org/10.1111/j.1095-8649.1988.tb05372.x.

Freeman, M., Eydal, M., Yoshimizu, M., Watanabe, K., Shinn, A., Miura, K., and Ogawa, K. (2011). Molecular identification and transmission studies of X-cell parasites from Atlantic cod Gadus morhua (Gadiformes: gadidae) and the northern black flounder Pseudopleuronectes obscurus (Pleuronectiformes: Pleuronectidae). Parasites Vectors *4*, 15. https://doi.org/10.1186/1756-3305-4-15.

Freeman, M.A. (2009). X-cell parasites in the European dab Limanda limanda are related to other X-cell organisms: a discussion on the potential identity of this new group of parasites. Parasitology *136*, 967–980. https://doi.org/10.1017/S0031182009006507.

Freeman, M.A., Fuss, J., Kristmundsson, Á., Bjorbækmo, M.F., Mangot, J.-F., del Campo, J., Keeling, P.J., Shalchian-Tabrizi, K., and Bass, D. (2017). X-cells are globally distributed, genetically divergent fish parasites related to Perkinsids and dinoflagellates. Curr. Biol. *27*, 1645–1651.e3. https://doi.org/10.1016/j.cub.2017.04.045.

Grange, L.J., and Smith, C.R. (2013). Megafaunal communities in rapidly warming fjords along the West antarctic Peninsula: hotspots of abundance and Beta diversity. PLoS One *8*, e77917. https://doi.org/10.1371/journal.pone.0077917.

Gutt, J., Isla, E., Xavier, J.C., Adams, B.J., Ahn, I.-Y., Cheng, C.C., Cheng, C.-H.C., Colesie, C., Cummings, V.J., di Prisco, G., et al. (2021). Antarctic ecosystems in transition – life between stresses and opportunities. Biol. Rev. *96*, 798–821. https://doi.org/10.1111/brv.12679.

Hillis, D.M., and Dixon, M.T. (1991). Ribosomal DNA: molecular evolution and phylogenetic inference. Q. Rev. Biol. *66*, 411–453. https://doi.org/10.1086/417338.

IPCC (2021). Climate Change 2021: The Physical Science Basis. Contribution of Working Group I to the Sixth Assessment Report of the Intergovernmental Panel on Climate Change (Cambridge University Press).

Itoïz, S., Metz, S., Derelle, E., Reñé, A., Garcés, E., Garcés, E., Bass, D., Soudant, P., and Chambouvet, A. (2022). Emerging parasitic Protists: the case of Perkinsea. Front. Microbiol. *12*, 735815. https://doi.org/10.3389/fmicb.2021.735815.

Kalyaanamoorthy, S., Minh, B.Q., Wong, T.K.F., von Haeseler, A., and Jermiin, L.S. (2017). ModelFinder: fast model selection for accurate phylogenetic estimates. Nat. Methods *14*, 587–589. https://doi.org/10.1038/nmeth.4285.

Karlsbakk, E., Nystøyl, C.F., Plarre, H., and Nylund, A. (2021). A novel protist parasite, Salmoxcellia vastator n. gen., n. sp. (Xcelliidae, Perkinsozoa), infecting farmed salmonids in Norway. Parasites Vectors *14*, 431. https://doi.org/10.1186/s13071-021-04886-0.

Katoh, K., Rozewicki, J., and Yamada, K.D. (2019). MAFFT online service: multiple sequence alignment, interactive sequence choice and visualization. Briefings Bioinf. *20*, 1160–1166. https://doi.org/10.1093/bib/bbx108.

Kim, B.-M., Amores, A., Kang, S., Ahn, D.-H., Kim, J.-H., Kim, I.-C., Lee, J.H., Lee, S.G., Lee, H., Lee, J., et al. (2019). Antarctic blackfin icefish genome reveals adaptations to extreme environments. Nat. Ecol. Evol. *3*, 469–478. https://doi.org/10.1038/s41559-019-0812-7.

Kozlov, A.M., Darriba, D., Flouri, T., Morel, B., and Stamatakis, A. (2019). RAxML-NG: a fast, scalable and user-friendly tool for maximum likelihood phylogenetic inference. Bioinformatics *35*, 4453–4455. https://doi.org/10.1093/bioinformatics/btz305.

Kraberger, S., Austin, C., Farkas, K., Desvignes, T., Postlethwait, J.H., Fontenele, R.S., Schmidlin, K., Bradley, R.W., Warzybok, P., Van Doorslaer, K., et al. (2022). Discovery of novel fish papillomaviruses: from the Antarctic to the

commercial fish market. Virology *565*, 65–72. https://doi.org/10.1016/j.virol.2021.10.007.

Mellergaard, S., and Nielsen, E. (1996). Epidemiology of X-cell gill disease in common dab Limanda limanda. Dis. Aquat. Org. *25*, 107–116. https://doi.org/10.3354/dao025107.

Menzel, P., Ng, K.L., and Krogh, A. (2016). Fast and sensitive taxonomic classification for metagenomics with Kaiju. Nat. Commun. *7*, 11257. https://doi.org/10.1038/ncomms11257.

Mesa, M.L., and Vacchi, M. (2001). Age and growth of high Antarctic notothenioid fish. Antarct. Sci. *13*, 227–235. https://doi.org/10.1017/S0954102001000335.

Miwa, S., and Kamaishi, T. (2009). X-cells in pseudotumors of yellowfin goby Acanthogobius flavimanus: a protistan organism distinct from that in flathead flounder Hippoglossoides dubius. Dis. Aquat. Org. *85*, 53–57. https://doi.org/10.3354/dao02058.

Morley, S.A., Abele, D., Barnes, D.K.A., Cárdenas, C.A., Cotté, C., Gutt, J., Henley, S.F., Höfer, J., Hughes, K.A., Martin, S.M., et al. (2020). Global drivers on Southern Ocean ecosystems: changing Physical environments and anthropogenic Pressures in an Earth system. Front. Mar. Sci. *7*, 1097. https://doi.org/10.3389/fmars.2020.547188.

Mühlfeld, C., Nyengaard, J.R., and Mayhew, T.M. (2010). A review of state-of-the-art stereology for better quantitative 3D morphology in cardiac research. Cardiovasc. Pathol. *19*, 65–82. https://doi.org/10.1016/j.carpath.2008.10.015.

Nurk, S., Meleshko, D., Korobeynikov, A., and Pevzner, P.A. (2017). metaSPAdes: a new versatile metagenomic assembler. Genome Res. *27*, 824–834. https://doi.org/10.1101/gr.213959.116.

Oksanen, J., Blanchet, F.G., Friendly, M., Kindt, R., Legendre, P., McGlinn, D., Minchin, P.R., O'Hara, R.B., Simpson, G.L., Solymos, P., et al. (2020). Vegan: community ecology package.

Paradis, E., and Schliep, K. (2019). Ape 5.0: an environment for modern phylogenetics and evolutionary analyses in R. Bioinformatics *35*, 526–528. https://doi.org/10.1093/bioinformatics/bty633.

Peck, L. (2018). Antarctic marine biodiversity: adaptations, environments and responses to change. In Oceanography and Marine Biology: An Annual Review, S.J. Hawkins, A.J. Evans, A.C. Dale, L.B. Firth, and I.P. Smith, eds. (Taylor and Francis), pp. 105–236.

Pinkerton, M.H., Boyd, P.W., Deppeler, S., Hayward, A., Höfer, J., and Moreau, S. (2021). Evidence for the impact of climate change on primary Producers in the Southern Ocean. Front. Ecol. Evol. *9*, 134. https://doi.org/10.3389/fevo.2021.592027.

Price, S.J., Leung, W.T.M., Owen, C.J., Puschendorf, R., Sergeant, C., Cunningham, A.A., Balloux, F., Garner, T.W.J., and Nichols, R.A. (2019). Effects of historic and projected climate change on the range and impacts of an emerging wildlife disease. Global Change Biol. *25*, 2648–2660. https://doi.org/10.1111/gcb.14651.

R Core Team (2017). R: A Language and Environment for Statistical Computing (Vienna, Austria: R Foundation for Statistical Computing).

R Studio Team (2020). RStudio: integrated development for R (RStudio, PBC).

Rye, C.D., Marshall, J., Kelley, M., Russell, G., Nazarenko, L.S., Kostov, Y., Schmidt, G.A., and Hansen, J. (2020). Antarctic glacial melt as a driver of recent Southern Ocean climate trends. Geophys. Res. Lett. *47*. e2019GL086892. https://doi.org/10.1029/2019GL086892.

Schneider, C.A., Rasband, W.S., and Eliceiri, K.W. (2012). NIH Image to ImageJ: 25 years of image analysis. Nat. Methods *9*, 671–675. https://doi.org/10.1038/nmeth.2089.

Silvano, A., Rintoul, S.R., Peña-Molino, B., Hobbs, W.R., van Wijk, E., Aoki, S., Tamura, T., and Williams, G.D. (2018). Freshening by glacial meltwater enhances melting of ice shelves and reduces formation of Antarctic Bottom Water. Sci. Adv. *4*, eaap9467. https://doi.org/10.1126/sciadv.aap9467.

Swart, N.C., Gille, S.T., Fyfe, J.C., and Gillett, N.P. (2018). Recent Southern Ocean warming and freshening driven by greenhouse gas emissions and ozone depletion. Nat. Geosci. *11*, 836–841. https://doi.org/10.1038/s41561-018-0226-1.

Van Doorslaer, K., Kraberger, S., Austin, C., Farkas, K., Bergeman, M., Paunil, E., Davison, W., and Varsani, A. (2018). Fish polyomaviruses beloDang to two distinct evolutionary lineages. J. Gen. Virol. *99*, 567–573. https://doi.org/10.1099/jgv.0.001041.

Wickham, H. (2011). ggplot2. WIREs Comput. Stat. *3*, 180–185. https://doi.org/10.1002/wics.147.

STAR★METHODS

KEY RESOURCES TABLE

REAGENT or RESOURCE	SOURCE	IDENTIFIER
Antibodies		
Anti-Digoxigenin-AP Fab fragments	Sigma-Aldrich	Cat# 11093274910, RRID:AB_2734716
Chemicals, peptides, and recombinant proteins		
Proteinase K	Qiagen	Cat# 19157
Denhardt's solution 50x	Sigma-Aldrich	Cat# D2532
Yeast rRNAs	Sigma-Aldrich	Cat# 10109223001
Triton X-100	Sigma-Aldrich	Cat# 11332481001
4-Nitro blue tetrazolium chloride (NBT)	Sigma-Aldrich	Cat# 11383213001
5-Bromo-4-chloro-3-indolyl-phosphate (BCIP)	Sigma-Aldrich	Cat# 10760994001
Nuclear Fast Red	Vector Laboratories	Cat# H-3403
Critical commercial assays		
High Pure Viral Nucleic Acid Kit	Roche Life Science	Cat# 11858874001
TruSeq DNA Nano Kit	Illumina	Cat# 20015964
Ribo-Zero Plus rRNA Depletion Kit	Illumina	Cat# 20040526
DNeasy Blood and tissue Kit	Qiagen	Cat# 69504
TruSeq Stranded Total RNA LT Kit	Illumina	Cat# 20020598
Deposited data		
Fish pictures and skin pathology of X-cell infection in *Trematomus scotti*	This paper	USAP-DC: https://doi.org/10.15784/601496
Morphological and pathological data of *Trematomus scotti* specimens captured on May 30th, 2018 in Andvord Bay	This paper	USAP-DC: https://doi.org/10.15784/601494
Histopathology of X-cell xenomas in *Trematomus scotti* and *Nototheniops larseni*	This paper	USAP-DC: https://doi.org/10.15784/601536
Raw Illumina sequencing reads from skin tumors and visually healthy skins from *Trematomus scotti* and *Nototheniops larseni*	This paper	NCBI SRA BioProject: PRJNA789574
Metagenomic analysis of apparently healthy and tumor samples using Kaiju software	This paper	USAP-DC: https://doi.org/10.15784/601537
Phylogenetic Analysis of *Notoxcellia* species	This paper	USAP-DC: https://doi.org/10.15784/601501
In situ hybridization of X-cell and host fish 18S SSU rRNA in alternate sections of tumor xenomas	This paper	USAP-DC: https://doi.org/10.15784/601539
MicroMRI and microCT images of *Trematomus scotti* with X-cell xenomas	This paper	MorphoSource: Project 000405843
microMRI analyses of *Trematomus scotti* Tsco_18_08 with X-cell xenomas	This paper	USAP-DC: https://doi.org/10.15784/601538
18 SSU rDNA type sequences for *Notoxcellia coronata* (nov. sp.) from *T. scotti*	This paper	NCBI GenBank: OL630144
18 SSU rDNA type sequences for *Notoxcellia picta* (nov. sp.) from *N. larseni*	This paper	NCBI GenBank: OL630145

(*Continued on next page*)

Continued

REAGENT or RESOURCE	SOURCE	IDENTIFIER
Temperature profiles at five fishing locations on the West Antarctic Peninsula during austral fall 2018	This paper	USAP-DC: https://doi.org/10.15784/601495
NCBI RefSeq nucleotide and protein databases	NCBI	Last accessed: July 24th, 2021
Oligonucleotides		
Custom HPLC-purified 5′ digoxygenin labelled DNA-Oligoprobe for 18S rRNAs of notothens: AGAGCATCGAGGAGGCGCCGAGAGGC	This paper	Genewiz
Custom HPLC-purified 5′ digoxygenin labelled DNA-Oligoprobe for 18S rRNAs of *Notoxcellia*: TAGGAATTCCTCGTTCAAGACG	This paper	Genewiz
Xcellidae 18s SSU rRNA Primer Pair1-Forward (18e_AllX): CTGGTTGATYCTGCCAGT	Adapted from (Hillis and Dixon, 1991)	IDT
Xcellidae 18s SSU rRNA Primer Pair1-Reverse (NLR-1300r_AllX): YCSTCCRATCCTCA GTCGG	Adapted from (Freeman, 2009)	IDT
Xcellidae 18s SSU rRNA Primer Pair2-Forward (18_Int_F1): CAGGCGCGTAAATTACCCAA	This paper	IDT
Xcellidae 18s SSU rRNA Primer Pair2-Reverse (18_Int_R1): CAGACAAATCGCTCCACCAA	This paper	IDT
Xcellidae 18s SSU rRNA Primer Pair3-Forward (18_Int_F2): TCAGATACCGTCGTAGTCCT	This paper	IDT
Xcellidae 18s SSU rRNA Primer Pair3-Reverse (18_Int_R2): AAAGGGCAGGGACGTAATCA	This paper	IDT
Xcellidae 18s SSU rRNA Primer Pair4-Forward (X-F1M_AllX): GYTCTTTCTTGATTYTATRRG	Adapted from (Freeman et al., 2017)	IDT
Xcellidae 18s SSU rRNA Primer Pair4-Reverse (18gMd): ATCCTTCYGCWGGTTCACCTAC	(Freeman et al., 2017)	IDT
Software and algorithms		
Trimmomatic v0.39	(Bolger et al., 2014)	http://www.usadellab.org/cms/?page=trimmomatic
metaSPAdes 3.14.0	(Nurk et al., 2017)	http://cab.spbu.ru/software/spades/
Kaiju v.1.7.4	(Menzel et al., 2016)	https://kaiju.binf.ku.dk/
vegan v.2.5-7 R package	(Oksanen et al., 2020)	https://cran.r-project.org/web/packages/vegan/index.html
ape v.5.4-1 R package	(Paradis and Schliep, 2019)	https://cran.r-project.org/web/packages/ape/index.html
ade4 v.1.7-16 R package	(Dray and Dufour, 2007)	https://cran.r-project.org/web/packages/ade4/index.html
ggplot2 package v.3.3.3	(Wickham, 2011)	https://cran.r-project.org/web/packages/ggplot2/index.html
MAFFT v.7.407	(Katoh et al., 2019)	https://mafft.cbrc.jp/alignment/software/
BMGE v.1.12	(Criscuolo and Gribaldo, 2010)	https://bioweb.pasteur.fr/packages/pack@BMGE@1.12
ModelFinder	(Kalyaanamoorthy et al., 2017)	http://www.iqtree.org/
RAxML-NG	(Kozlov et al., 2019)	https://github.com/amkozlov/raxml-ng
ImageJ 1.50e	(Schneider et al., 2012)	https://imagej.nih.gov/ij/index.html

(*Continued on next page*)

Continued

REAGENT or RESOURCE	SOURCE	IDENTIFIER
Multipurpose Grid ImageJ macro v.0.1, 14/08/2011	Aleksandr Mironov	https://imagej.nih.gov/ij/macros/Multipurpose_grid.txt
Amira 5.6	FEI, Visualization Sciences Group	https://www.thermofisher.com/us/en/home/electron-microscopy/products/software-em-3d-vis/amira-software.html
Adobe Acrobat 3D v8 Toolkit	Adobe	N/A
R software v.4.0.3	(R Core Team, 2017)	https://www.r-project.org/
RStudio v.1.3.1093	(R Studio Team, 2020)	https://www.rstudio.com/
Other		
ZooBank registration of the new genus *Notoxcellia*	This paper	ZooBank: LSID: urn:lsid:zoobank.org:act:5CF9609E-0111-4386-8518-BD50B5BDDE0E
ZooBank registration of the species *Notoxcellia coronata*	This paper	ZooBank: LSID: urn:lsid:zoobank.org:act:194D91B2-E268-4238-89E2-385819F2C35B
ZooBank registration of the species *Notoxcellia picta*	This paper	ZooBank: LSID: urn:lsid:zoobank.org:act:31062DD2-7202-47FA-86E0-7BE5C55AC0E2
Notoxcellia coronata DNA extracts from type specimens Trematomus_scotti_18_02 (holotype), and Tsco_18_05-07, and 11 (paratypes)	This paper	Zoological Museum, University of Copenhagen, ZMUC P2397603-P2397607
Notoxcellia coronata histopathology sections of X-cell xenomas in Trematomus_s-cotti_18_02 (holotype) and Tsco_18_05 and 11 (paratypes)	This paper	Zoological Museum, University of Copenhagen, ZMUC P2398903-P2398906
Trematomus scotti specimens (Tsco_18_8-10) infected by *Notoxcellia coronata*	This paper	Zoological Museum, University of Copenhagen, ZMUC P241299-P241301
Notoxcellia picta DNA extracts from type specimen Nototheniops_larseni_18_110 (holotype)	This paper	Zoological Museum, University of Copenhagen, ZMUC P2397608
Notoxcellia picta histopathology sections of X-cell xenomas in Nototheniops_lar-seni_18_110 (holotype)	This paper	Zoological Museum, University of Copenhagen, ZMUC P2397609- P2397610

RESOURCE AVAILABILITY

Lead contact

Further information and requests for resources and reagents should be directed to and will be fulfilled by the lead contact, Thomas Desvignes (tdesvign@uoregon.edu).

Materials availability

This study did not generate new unique reagents.

Data and code availability

- All data have been deposited at NCBI GenBank: OL630144 and OL630145, NCBI SRA BioProject: PRJNA789574, at MorphoSource Project: 000405843, and at USAP-DC Project: p0010221, and are publicly available as of the date of publication. Biological materials have been deposited at the Zoological Museum of the University of Copenhagen. Additional accession numbers and DOIs are listed in the key resources.
- This paper does not report original code.
- Any additional information required to reanalyze the data reported in this paper is available from the lead contact upon request.

EXPERIMENTAL MODEL AND SUBJECT DETAILS

Research fishing operations were conducted at various locations on the West Antarctic Peninsula from May to June 2018 (Figure S9) on board the Antarctic Research and Supply Vessel (ARSV) *Laurence M. Gould* using an 18-ft otter trawl equipped with a rockhopper gear. Crowned notothen *T. scotti* specimens, with and without tumors, were all captured during two 20-min bottom-time trawls performed on the night of May 29th to May 30th, 2018, in Andvord Bay (64º50'S-62º39'W) at a depth of ~380–400 m. More than 300 crowned notothen were captured in the two tows. Noticing the severe tumors in crowned notothens immediately after recovery of both trawls, we decided not to collect all diseased specimens due to concerns about transporting potentially contagious pathogens to the aquarium facilities at Palmer Station and its surrounding environment. We retained, however, a random subset of 90 adult specimens of various sizes, of which 24 (27%) had tumors of varying degrees of severity and 66 (73%) were apparently healthy, and maintained them in flow-through seawater aquaria on board the research vessel. All other specimens were released alive at the site of collection. Our selection of specimens was not motivated by any criteria, but it is possible that we unconsciously biased our sampling towards either larger specimens or severely affected specimens. Therefore, our sampling may not precisely reflect the prevalence of tumors in the population. Fish were transported live to Palmer Station on Anvers Island, Antarctica. Apparently healthy specimens were kept in the aquarium flow-through system at ~0ºC while visually diseased fish were kept isolated in aquaria and euthanized within 24 h of arrival at the research station.

Each *T. scotti* specimen was euthanized by an overdose of Tricaine-S (MS 222, Syndel) followed by the sectioning of the spinal cord just behind the head after morphometric measurements were taken. The standard length (SL) of each specimen was measured to the nearest millimeter and the total weight (W) recorded to the nearest 0.1 gram. Each specimen was carefully inspected for external signs of disease and classified as "healthy" or "diseased". We photographed the left side of each healthy fish and both sides of each diseased fish. The sex of each specimen was recorded at dissection based on gonad morphology. When the sex could not be determined, the individual was recorded as "ambiguous". Pictures, morphometric and sex data for *T. scotti* specimens are available in the United States Antarctic Program Data Center (USAP-DC Project p0010221). Tumor fragments from five diseased crowned notothens were sampled in 70% ethanol for DNA analyses, in Bouin's fixative for histopathological analyses, and in 4% PFA overnight followed by progressive dehydration and storage in 100% methanol for *in situ* hybridization analyses. Matching control samples were made from five apparently healthy specimens. Three specimens of crowned notothen displaying severe tumors were fixed in 4% neutral buffered formalin for seven days, then rinsed and preserved in 70% ethanol for microCT and microMRI analyses.

A diseased specimen of painted notothen *N. larseni* with a large skin tumor located under the head and between the pelvic fins, was captured during a 20-min bottom-time trawl performed on the night of June 5th to June 6th, 2018, in the north part of Dallmann Bay (63º55'S-62º46'W) at a depth of ~180 m. Although 116 painted notothens were sampled this season, several hundred individuals of this common species were captured during our 2018 field campaign, and most were released alive on site of capture. Only one specimen, however, was noticed to be visibly affected by skin tumors. Thus, the prevalence of skin disease in the sampled painted notothen population was much lower than in the crowned notothen population in Andvord Bay. Samples from the diseased painted notothen specimen (Nlar_18_110, SL = 14.7 cm, W = 31.8 g) and a paired control (Nlar_18_111, SL = 16.8 cm, W = 49.2 g) were performed as described for crowned notothens.

All procedures on animals were performed following IACUC protocol #13-27RRAA approved by the University of Oregon, and access to Antarctic Specially Protected Areas 152 (Western Bransfield Strait) and 153 (Eastern Dallmann Bay) for fishing was authorized by the Antarctic Conservation Act Permit ACA 2016-025.

METHOD DETAILS

Metagenomic analysis

Skin tumor samples from five crowned notothen *T. scotti* and one painted notothen *N. larseni* and apparently healthy skin samples from five crowned notothens and one painted notothen without visible tumors were processed for DNA and RNA metagenomic analyses. Tissue samples stored in ethanol were first air dried under sterile conditions in a laminar flow hood to remove traces of ethanol. Samples were then homogenized in 400 μL of SM buffer (50 mM Tris–HCl, 10 mM $MgSO_4$, 0.1 M NaCl, pH 7.5). Homogenates (200 μL) were enriched for viral DNA and RNA using the High Pure Viral nucleic acid Kit (Roche Diagnostics,

USA). Resulting DNA and RNA samples were used to prepare 2 × 150 bp libraries using TruSeq Nano DNA kit (Illumina, USA) and TruSeq Stranded Total RNA LT Kit with Ribo-Zero Human/Mouse/Rat (Illumina, USA). The 2 × 150 bp libraries were sequenced on an Illumina NovaSeq6000 sequencer at Psomagen Inc. (USA). Raw reads were deposited in NCBI SRA under BioProject PRJNA789574.

Demultiplexed reads were trimmed using Trimmomatic v0.39 (Bolger et al., 2014) and *de novo* assembled using metaSPAdes (k = 33, 55, 77) 3.14.0 (Nurk et al., 2017). Resulting contigs >750 nts were analyzed against the NCBI RefSeq viral protein database to identify viral-like sequences using blastx. Each library was further analyzed with Kaiju v.1.7.4 (Menzel et al., 2016) using a custom database generated from the NCBI NR database retrieved on July 24th, 2021, and containing all viruses, archaea, and bacteria sequences, as well as microbial eukaryotes and *Trematomus* spp. fish sequences (available in the United States Antarctic Program Data Center USAP-DC Project p0010221). Kaiju was run in default mode and outputs of the analysis of each sequencing library were converted to taxonomic levels using the function *kaiju2table* (Output files available in the United States Antarctic Program Data Center USAP-DC Project p0010221). Taxonomically classified contigs were further analyzed using Bray-Curtis dissimilarity in the *vegan* v.2.5-7 package (Oksanen et al., 2020) and plotted in a non-scaled principal coordinates analysis (PCoA) using the *ape* v.5.4-1 (Paradis and Schliep, 2019) and *ade4* v.1.7-16 (Dray and Dufour, 2007, p. 4) packages.

Histopathology

Fresh tumorous and healthy skin samples were preserved in Bouin's fixative until histological processing. Briefly, fixed samples were thoroughly washed in 70% ethanol, embedded in paraffin wax, and sectioned at 3–5 μm. Sections were then stained with hematoxylin and eosin (H & E). Observations were performed under a Leica DMLB® compound light microscope equipped with a SPOT RT® color camera (Diagnostic Instruments) interfaced to an IBM compatible computer with SPOT RT® image capture software v3.0 (Diagnostic Instruments). Additional histopathology pictures for *T. scotti* and *N. larseni* specimens are available in the United States Antarctic Program Data Center (USAP-DC Project p0010221).

PCR amplifications

DNA was extracted from the same sample sets used for the metagenomic analysis using the Qiagen DNeasy Blood and tissue kit (Hilden, Germany). DNA concentrations were measured with a Qubit 3 fluorometer, and 2 ng of DNA was used as input for each PCR reaction. PCR amplification of X-cell 18S rRNA small subunit (18S SSU rRNA) fragments were performed at the annealing temperature of 55ºC, 40 cycles of PCR using the primers presented in Figure 2 and Data S2. Amplification of the notothenioid fish mitochondrial marker *cytochrome c oxidase I, mitochondrial* (*mt-co1*) was performed as previously described (Desvignes et al., 2019). PCR amplification accuracy was verified by sequencing PCR products in both directions at GENEWIZ (Cambridge, MA, USA) followed by BLAST searches in the NCBI nucleotide database.

Phylogenetic tree reconstruction

For phylogenetic tree reconstruction, we gathered sequences previously used to decipher the phylogenetic position of the *Xcellidae* family in the superphylum Alveolata (Freeman et al., 2017). The NCBI nucleotide database was searched for newly added, representative sequences from *Xcellidae* and from all sister lineages of the phylum Perkinsozoa, which includes *Perkinsus* spp., *Parvilucifera* spp., *Snorkelia* sp., *Tuberlatum coatsi*, and *Dinovorax pyriformis*. Several undescribed alveolate lineages not belonging to *Xcellidae* were excluded from subsequent analyses. Combined sequences were aligned with MAFFT v.7.407 using the E-INS-i algorithm and otherwise default parameters (Katoh et al., 2019). The resulting alignment was visually corrected and further curated with BMGE v.1.12 with default parameters (Criscuolo and Gribaldo, 2010). The optimal Maximum likelihood substitution model was searched using ModelFinder and selected based on the Bayesian Information Criterion (BIC) (Kalyaanamoorthy et al., 2017). The phylogenetic tree was then reconstructed using RAxML-NG (Kozlov et al., 2019), with the model GTR + F + I + G4 for the Alveolate tree and the model TIM3+F + G4 for the tree focused on *Xcellidae*, and an initial tree search of 100 parsimony and 100 random trees, followed by 200 bootstraps. Alignments and tree files are available in the United States Antarctic Program Data Center (USAP-DC Project p0010221).

In situ hybridization

In situ hybridization experiments were carried out using HPLC-purified 5′ digoxygenin labelled DNA-Oligoprobes designed to specifically bind 18S rRNAs of notothens (AGAGCATCGAGGAGGCGCCGAG AGGC) or *Notoxcellia* (TAGGAATTCCTCGTTCAAGACG) (Genewiz, Cambridge, MA, USA). The *in situ* hybridization protocol was extensively adapted from the protocol described by Freeman (2009), which started with sections of formaldehyde fixed samples embedded in paraffin.

In detail, samples fixed with 4% paraformaldehyde (PFA) and stored at −20ºC in 100% methanol were rehydrated and processed for cryosectioning at 15 μm. Serial sections were deposited on alternate slides, air dried, and stored at −20 ºC until *in situ* hybridization as follows. First, the sections were rehydrated in TBS pH 8.0 (50 mM Tris pH 8.0 and 150mM NaCl) for 5 min at room temperature (RT), encircled with PAP-pen, and permeabilized with Proteinase K (Qiagen) in TBS pH 8.0 for 25 min at 37 ºC. After a few trials, we selected optimal Proteinase K concentrations for each subsequent probe (20 μg mL^{-1} for the notothen probe and 40 μg mL^{-1} for the *Notoxcellia* probe). After washes in phosphate-buffered saline (PBS) at RT, sections were post-fixed with 0.4% PFA in PBS for 15 min at RT followed by a wash in distilled water. To prevent non-specific peroxidase binding, sections were covered with 10% H_2O_2 in methanol for 10 min at RT, rinsed with distilled water, and air dried at 45 ºC. Species-specific probes were diluted in hybridization buffer (2× SSC, 1× Denhardt's solution, 200 μg mL^{-1} of yeast rRNA in TBS pH 8.0) at concentrations of 0.5 μM for the notothen probe and 2 μM for the *Notoxcellia* probe and denatured for 5 min at 95 ºC. The hybridization solution containing probe was dispensed on the sections, cover slipped, and hybridized for 2 h at 45 ºC in a humid chamber with 2× SSC. Slides were subsequently washed in 2× SSC and in 0.1× SSC with 0.25% Tween-20. After equilibration in Genius Buffer (100 mM Tris pH 7.5 and 150 mM NaCl) for 10 min at RT, slides were incubated with blocking solution (2% sheep serum and 0.1% triton X-100 in Genius Buffer) for 1 h at RT. Immunological detection was carried out on slides with AP-conjugated Fab fragments from anti-DIG sheep antiserum diluted at 1:3,000 in blocking solution and incubated overnight (18–20 h) at RT in a wet chamber. Slides were thoroughly washed with blocking solution at RT to remove residual Fab fragments (2 × 10-min and 3 × 20-min washes in a Coplin jar on an orbital shaker set at 5 rotations per minute) and then transferred into washing buffer (100 mM Tris pH 9.5, 100 mM NaCl, and 50 mM $MgCl_2$) at RT. Colorimetric reactions were performed on slides, in the dark, at RT with nitro blue tetrazolium and 5-bromo-4-chloro-3-indolyl phosphate (NBT and BCIP at 4.5 μL mL^{-1} and 3.5 μL mL^{-1}, respectively, in washing buffer) in a wet chamber humidified with washing buffer. Colorimetric reactions were allowed to progress until the desired intensity was reached (about 1.5 h for the notothen probe and 4 h for the *Notoxcellia* probe) and stopped by washes in distilled water at RT in Coplin jars. Slides were then counterstained with Nuclear Fast Red for 8 min at RT, washed for 3 min in 95% ethanol and 2 × 3 min in 100% ethanol, cleared in xylene, and mounted with Permount Mounting Medium. Resulting stained sections were observed on a Leica DMLB microscope and captured with a Leica DFC310 FX camera controlled by the Leica Application Suite X (LAS X). Additional *in situ* hybridization pictures for *T. scotti* and *N. larseni* samples using the fish or the X-cell probe are available in the United States Antarctic Program Data Center (USAP-DC Project p0010221).

Surface analysis

Photographs of both left and right sides of crowned notothens exhibiting skin lesions were used to quantify the fish surface area (fin and eye surfaces excluded) affected by the *Notoxcellia* parasite. Of the 24 specimens of crowned notothen with tumors, 21 were quantified using ImageJ 1.50e (Schneider et al., 2012). Three other specimens lacked images for both sides, or the images were too dark to be analyzed. For each specimen, a rough region of interest covering the left surface area was first drawn to estimate the surface area of the specimen. This surface area estimate was used to superimpose a randomized point grid (*Multipurpose Grid* macro v.0.1, 14/08/2011 Aleksandr Mironov) on both the left- and right-side photos with a grid size providing ~200 points on the surface of each side of the fish. The ImageJ cell counter plugin was used to count and document all intersections of randomized points with underlying surface structures. The skin phenotype was categorized as 1, seemingly healthy skin (no apparent infection by the parasites); 2, moderately affected skin (unnatural skin color, most often reddish or yellowish); and 3, severely affected skin (bloody wound or pronounced raised surface). The fraction of randomized points that intersected with each underlying skin category represents the fraction of the total surface area for that category. Because the three-dimensional geometric shape of the fish is not flat nor represented by a cube, but rather by an elliptic cylinder, the photography-based approach estimates the projected surface area and will, to a small degree, underestimate true surface area in dorsal- and ventral-most regions.

Subsequently, the manually segmented point grids for each skin category were averaged between left and mirrored right side for each fish and then averaged over all 21 specimens to generate prevalence heatmaps for the distribution of moderately affected skin, severely affected skin, and total affected skin. Because all specimens were horizontally aligned on the images and the generation of ~200 points per side ruled out size differences, this approach yielded average heatmaps with minimal outline distortion. Raw and analyzed images files are available in the United States Antarctic Program Data Center (USAP-DC Project p0010221).

microMRI and microCT analyses

To image internal features of the tumors, one crowned notothen specimen (Tsco_18_08, $BM_{n=1}$ = 43.0 g, $SL_{n=1}$ = 13.5 cm) was used for high-field micro magnetic resonance imaging. The same specimen and two additional specimens (Tsco_18_09 and Tsco_18_10, $BM_{n=3}$ = 45.5 ± 26.1 g, $SL_{n=3}$ = 13.7 ± 2.7 cm) were used for diffusible iodine-based contrast-enhanced micro computed tomography.

Before microMRI imaging, the tail fin of the Tsco_18_08 specimen was removed so that the specimen could fit in the analytical tube. The specimen was then placed in a 50 mL Falcon tube and immersed in Fomblin Y, a H^+-devoid medium providing completely dark background in H^+-MRI, under a low vacuum to extract air bubbles. Magnetic resonance imaging was performed on an Agilent 9.4 T system equipped with a Rapid-40-H^+ body coil and using a 3D gradient echo sequence with the following parameters: repetition time = 19 ms, echo time = 5.464 ms, flip angle = 30°, field-of-view = 50 × 50 × 50 mm^3, spatial resolution 0.0651 mm isotropic, number of averages = 20, total acquisition time = 65 h. Two subsequent scans were performed to image both the head and the tail tumors of this specimen.

Before microCT imaging, fish specimens were stained in Lugol's solution (8.3 g L^{-1} of I_2 and 16.6 g L^{-1} KI) for one week with rocking. MicroCT scans were performed using a Scanco Medical XtremeCT system with the following parameters: X-ray tube voltage = 59.4 kVp, X-ray tube current = 119 μA, number of projections pr. 180° = 1,000, integration time = 132 ms, field-of-view = 70 × 70 × 70 mm^3, spatial resolution = 0.041 mm. MicroMRI and microCT images are available in MorphoSource Project 000405843.

Resulting microMRI and microCT images were analyzed with Amira 5.6 (FEI, Visualization Sciences Group) for segmentation and interactive pdf models (available in USAP-DC Project p0010221) were generated using Adobe Acrobat 3D v8 Toolkit.

Volume fraction of tumors relative to the total body volume of the specimen was based on the microCT data using stereological principles as described by Mühlfeld et al. (2010). In short, volume fraction was estimated by choosing 15 equally spaced parallel transversal sections spanning the entire body and applying a systematic uniform point grid on each section plane. Volume fraction was calculated by counting the number of test points intersecting either tumors or body using the Cavalieri estimator.

Morphometric analyses

Using the standard length (SL, cm) and total weight (W, g) of each specimen (available in USAP-DC Project p0010221), we analyzed the length-weight relationship and Fulton's Condition factor (*K*) of healthy and diseased fish. We first tested the effect of SL, sex, and tumor as a binary trait (presence/absence) and all their interactions on W. This full model was pruned in a step-wise manner until only factors significantly affecting the weight were retained. The quality of the resulting model was validated by the Akaike Information Criterion (AIC) and Bayesian Information Criterion (BIC) (Data S4A). Only SL and the tumor status variables were significant factors in the length-weight relationship. Linear regressions were then applied separately to the length-weight relationships of visually healthy and diseased specimens. Regression coefficients were used to derive growth models for the healthy and diseased crowned notothen in Andvord bay. The growth model of healthy specimens was used to calculate the deviation of tumor fish from their expected weight (Deviation = $W_{Measured}/W_{Expected}$ * 100). The growth coefficient of healthy crowned notothens (*b* = 3.27) was significantly different (*t-test*, t = 2.88, df = 64, p = 0.0054) from 3.0, which characterizes isometric growth, thus crowned notothens in Andvord Bay displayed an allometric growth. The growth coefficient estimated for the healthy fish was therefore used to adjust *K* for both healthy and diseased fish ($K = 100 \times W \times SL^{-b}$). We verified that SL, percentage of severely affected skin, and percentage of moderately plus severely affected skin were not correlated with *K*. Finally, we compared *K* of healthy and diseased fish using a one-sided t-test after verifying applicability using Levene's and Shapiro tests. These analyses

were repeated using the tumor factor as a continuous variable defined by percentages of body surface affected by the parasites (see Surface analysis) (Datas S4B and S4C). All statistical analyses were performed using R software v.4.0.3 (R Core Team, 2017) through RStudio v.1.3.1093 (R Studio Team, 2020) and graphs were generated using *ggplot2* package v.3.3.3 (Wickham, 2011).

QUANTIFICATION AND STATISTICAL ANALYSIS

Details of statistical analysis are provided within the relevant figure legends, their legends, and associated detailed methods. All statistical analyses were performed using R v4.0.3 (R Core Team, 2017) through RStudio v.1.3.1093 (R Studio Team, 2020). Metagenomic analyses (n = 6 "healthy" and n = 6 "tumor") were performed with Kaiju v.1.7.4 (Menzel et al., 2016) using a custom database. Taxonomic levels were obtained using the function *kaiju2table* and taxonomically classified contigs were analyzed using Bray-Curtis dissimilarity in the *vegan* v.2.5-7 package (Oksanen et al., 2020) and plotted in a non-scaled principal coordinates analysis (PCoA) using the *ape* v.5.4-1 (Paradis and Schliep, 2019) and *ade4* v.1.7-16 (Dray and Dufour, 2007) packages. Surface analysis was performed on 21 specimens of crowned notothen with tumors using ImageJ 1.50e (Schneider et al., 2012) and the *Multipurpose Grid* macro v.0.1, 14/08/2011 (Aleksandr Mironov) with a grid size providing ~200 points per side of the fish. Statistical difference in skin pathology between left and right sides of the fish was assessed using a two-sided paired Student's t-test. Segmented point grids for each category were averaged between left and mirrored right side for each fish and over all the 21 specimens to generate prevalence heatmaps. Growth models of healthy (n = 66) and diseased fish (n = 23) were analyzed by pruning in a step-wise manner a model testing the effect on weight of the length, sex, and tumor as a binary trait (presence/absence) and all their interactions. The quality of the resulting model was validated by Akaike Information Criterion (AIC) and Bayesian Information Criterion (BIC). Linear regressions were applied separately to the length-weight relationships of visually healthy and diseased specimens. Deviation of the growth coefficient from isometric growth (i.e., b = 3) was assessed using a two-sided Student's t-test, with significance set at $p \leq 0.05$. Growth coefficient estimates were used to adjust the condition factor K for both healthy and diseased fish ($K = 100 \times W \times SL^{-b}$) and calculate the deviation from expected weight. Hypothesizing that parasite infection has detrimental effects on the fish, K and deviation from expected weight of healthy and diseased fish were compared using a one-sided Student's t-test. These analyses were repeated using the tumor factor as a continuous variable defined by percentages of body surface affected by the parasites. Boxplots in Figures 4L and 4M represent the median, 25th and 75th percentiles, and 1.5x IQR. The dots plotted within figures represent individual data points.